Accuracy Assessment of Reduced-and Full-Order Virtual Synchronous Generator Models Under Different Grid Strength Cases

Yu, Yun; Chaudhary, Sanjay K.; Matas, Jose; Xu, Luona; Agundis Tinajero, Gibran David; Vasquez, Juan C.; Guerrero, Josep M.

Published in:
IECON 2022 - 48th Annual Conference of the IEEE Industrial Electronics Society

DOI (link to publication from Publisher):
10.1109/IECON49645.2022.9968830

Publication date:
2022

Document Version
Accepted author manuscript, peer reviewed version

Accuracy Assessment of Reduced- and Full-Order Virtual Synchronous Generator Models Under Different Grid Strength Cases

Yun Yu*, Sanjay K Chaudhary*, Jose Matas†, Luona Xu*, Gibran David Agundis Tinajero*,
Juan C. Vasquez* and Josep M. Guerrero*
*AAU Energy, Aalborg University, Aalborg, Denmark
†Department of Electrical Engineering, Polytechnic University of Catalonia, Barcelona, Spain
Email: *yyu@energy.aau.dk, *skc@energy.aau.dk, †jose.matas@upc.edu, *lxu@energy.aau.dk,
*gdat@energy.aau.dk, *juq@energy.aau.dk, *joz@energy.aau.dk

***Abstract*—The virtual synchronous generator (VSG) has been extensively applied for the integration of distributed generators. For the benefit of analysis, both the reduced-order small-signal model (RSM) and full-order small-signal model (FSM) have been proposed; however, because of the different modeling approaches, the modeling accuracy may differ a lot. To provide a guideline for selecting a suitable model, an accuracy assessment has been conducted in this paper, where different grid strength cases and equilibrium points are considered. More specific, the eigenvalue analysis is adopted for comparing the dominant dynamics of the RSM and FSM. Afterwards, the responses of the RSM and FSM are compared with the nonlinear model (NM) in the Digsilent/Powerfactory to show the modeling accuracy. It has been found that the RSM is mainly suitable for the weak and relatively strong grids, while the FSM shows better accuracy in the case of an extremely strong grid and around the equilibrium point that is close to VSG's rated output.**

***Keywords*—Small-signal model, short circuit ratio (SCR), virtual synchronous generator (VSG)**

I. Introduction

In the last decades, the distributed energy generation technology has been extensively developed. On the other hand, due to the increased penetration level of the electronic-based resources, the inertial level is inevitably degraded. As a consequence, maintaining the frequency stability becomes difficult [1]. To handle this issue, the grid-forming control has been proposed for the integration of distributed generators, of which the VSG is one of the most commonly used grid-forming algorithms [2]–[5].

For the analysis of the VSG, both RSM and FSM have been proposed in the literature. For example, the generalized droop control has been developed in [6], where the analysis was applied on the basis of VSG's decoupled RSM. The same modeling principle was adopted when different damping-level-correction algorithms were developed in [7]–[9]. In the case of analyzing a microgrid with several VSGs, the decoupled RSM was adopted in [10]. One problem of the decoupled RSM is that the coupling effects between VSG's active power control (APC) and reactive power control (RPC) are not considered, which may lead to an inaccurate analysis. Considering this, the RSM with the coupling terms was proposed in [11]. Using the RSM with coupling terms, the guideline for tuning VSG's APC and RPC was proposed by Wu et al. [11].

Although the RSM is able to show VSG's dominant dynamics, it still fails to include the complete dynamics. Moreover, using the RSM, it is impossible to analyze and tune VSG's inner current and voltage control loops. Thus, the FSM has been developed for the applications that need to consider all the dynamics [12]–[14]. For instance, an eigenvalue-sensitivity-based automatic tuning algorithm was developed by D'Arco et al. using the FSM approach [12]. In addition, using the FSM, Dong et al. analyzed the impact of current and voltage control parameters on VSG's stability [13], and a quantitative tuning guideline was presented. Qu et al. investigated the influences of the bandwidth of current and voltage control on VSG's stability and dynamics of the APC and RPC [14].

It is well-known that the RSM is advanced in providing a simple and straightforward analysis because the modeling can be directly applied by using the phasor representation. On the other hand, the FSM performs better in providing more stability information since it includes the complete dynamics. However, at a cost of that, the modeling complexity and computation burden will inevitably increase. For distributed generators, the grid strength has a notable impact on the control stability. As it was found in [14], under different grid strength cases, the damping level of VSG's APC and RPC vary significantly. Considering this, an accuracy assessment of the RSM and FSM is conducted in this paper to figure out how the grid strength affects the modeling accuracy, which provides a guideline for selecting a suitable model.

The rest of this paper is organized as following: In Section II, the VSG to be studied is introduced. Then, the RSM with coupling terms and the FSM are derived. In Section III, an assessment of the modeling accuracy is applied with the help of the eigenvalue analysis and simulation studies. In Section IV, the discussion and conclusion are given.

This work was supported partly by VILLUM FONDEN under the VILLUM Investigator Grant (No. 25920), partly by Ministry of Foreign Affairs of Denmark, partly by Danida Fellowship Centre (No. 19-M03-AAU) and partly by China Scholarship Council.

II. Small-Signal Modeling of the VSG

In this paper, a typical VSG control frame as Fig. 1 is used for deriving the small-signal models. As shown in Fig. 1, the VSG is applied with the virtual impedance and the cascaded current and voltage control. The active power is then regulated by the conventional swing equation, and the reactive power is managed by a PI controller.

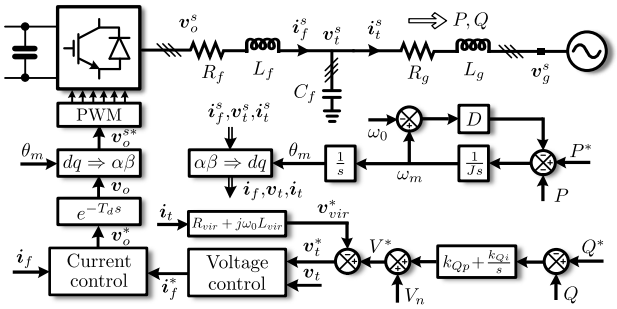

Figure 1. Simplified diagram of a grid-tied VSG.

A. Reduced-Order Small-Signal Model (RSM)

Firstly, the assumption that the switching frequency is high enough to guarantee a high control bandwidth is normally applied. Then, the inner current and voltage control loops can be excluded from the modeling. Only the virtual impedance, APC and RPC are included in the analysis, and the VSG is simplified to a phasor representation, as shown in Fig. 2.

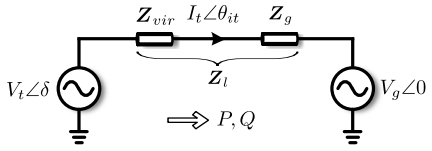

Figure 2. Phasor representation of the VSG.

In Fig. 2, $\boldsymbol{Z}_l$ is the equivalent grid impedance which is the sum of the virtual impedance $\boldsymbol{Z}_{vir}$ and real grid impedance $\boldsymbol{Z}_g$; $V_t\angle\delta$, $I_t\angle\theta_{it}$ and $V_g\angle 0$ represent the capacitor voltage, grid-side current and grid voltage phasors, respectively; The voltage angle δ is formulated as

$$\delta = \int (\omega_m - \omega_g)\, dt \tag{1}$$

where ω_m and ω_g denote angular frequencies of the VSG and grid voltage, respectively.

Assuming $\boldsymbol{Z}_l$ is mainly inductive, we have $\boldsymbol{Z}_l \approx X_l$. From Fig. 2, the power formula is written as

$$\boldsymbol{S} = P + jQ = 3\frac{V_t V_g \sin\delta}{2X_l} + j3\frac{V_t^2 - V_t V_g \cos\delta}{2X_l}. \tag{2}$$

The power perturbations can be then expressed as

$$\Delta\boldsymbol{S} = \frac{\partial \boldsymbol{S}}{\partial\delta}\Delta\delta + \frac{\partial \boldsymbol{S}}{\partial V_t}\Delta V_t + \frac{\partial \boldsymbol{S}}{\partial V_g}\Delta V_g. \tag{3}$$

Approximately, $\sin\delta \approx \delta$, $\cos\delta \approx 1$ and $V_t \approx V_g \approx V_n$. The grid is normally taken as a infinite bus that $\Delta V_g \approx 0$.

Subsequently, power perturbations are derived from (3) as

$$\Delta P = \frac{3V_n^2}{2X_l}\Delta\delta + \frac{3V_n\delta_n}{2X_l}\Delta V_t, \tag{4}$$

$$\Delta Q = \frac{3V_n}{2X_l}\Delta V_t + \frac{3V_n^2\delta_n}{2X_l}\Delta V_t \tag{5}$$

where δ_n is the static power angle.

From Fig. 1, we have VSG's APC law as

$$P^* - P = J\frac{d\omega_m}{dt} + D\left(\omega_m - \omega_0\right) \tag{6}$$

where P^* and P are the active power set point and feedback; ω_0 denotes the nominal angular frequency; J and D represent the inertia and damping constants, respectively.

VSG's RPC law is formulated as

$$V^* = (Q^* - Q)\left(k_{Qp} + \frac{k_{Qi}}{s}\right) + V_n \tag{7}$$

where V^* is the voltage amplitude set point; Q^* and Q are the reactive power set point and feedback; k_{Qp} and k_{Qi} are the PI control parameters; V_n denotes the nominal voltage amplitude.

Substituting (4) and (5) into the small-signal expressions of (1), (6) and (7), VSG's RSM is derived as

$$\frac{\Delta P}{\Delta P^*} = \frac{\frac{k_a G_P(s)}{s}\left[1 - \frac{k_b G_Q(s)}{1+k_b G_Q(s)}\delta_n^2\right]}{1 + \frac{k_a G_P(s)}{s}\left[1 - \frac{k_b G_Q(s)}{1+k_b G_Q(s)}\delta_n^2\right]}, \tag{8}$$

$$\frac{\Delta Q}{\Delta Q^*} = \frac{k_b G_Q(s)\left[1 - \frac{k_a G_P(s)}{1+k_a G_P(s)}\delta_n^2\right]}{1 + k_b G_Q(s)\left[1 - \frac{k_a G_P(s)}{1+k_a G_P(s)}\delta_n^2\right]} \tag{9}$$

where k_a, k_b, $G_P(s)$ and $G_Q(s)$ are

$$k_a = \frac{3V_n^2}{2X_l}, k_b = \frac{3V_n}{2X_l}, G_P(s) = \frac{1}{Js + D}, G_Q(s) = k_{Qp} + \frac{k_{Qi}}{s}. \tag{10}$$

B. Full-Order Small-Signal Model (FSM)

Different from VSG's RMS which only considers the APC and RPC, the FSM includes the effects of the control delay and cascaded current and voltage control as well.

1) LC filter: Firstly, the passive LC filter which is used as the grid interface is modeled. Let $\boldsymbol{v}_o$, $\boldsymbol{i}_f$, $\boldsymbol{v}_t$, $\boldsymbol{i}_t$ and $\boldsymbol{v}_g$, respectively, denote the inverter output, inverter-side current, capacitor voltage, grid-side current and grid voltage vectors. The dynamics of the LC filters are expressed by the differential equations in the dq coordinates as follows:

$$\boldsymbol{v}_o = R_f\boldsymbol{i}_f + L_f\frac{d\boldsymbol{i}_f}{dt} + j\omega_m L_f\boldsymbol{i}_f + \boldsymbol{v}_t, \tag{11}$$

$$\boldsymbol{i}_f = C_f\frac{d\boldsymbol{v}_t}{dt} + j\omega_m C_f\boldsymbol{v}_t + \boldsymbol{i}_t, \tag{12}$$

$$\boldsymbol{v}_t = R_g\boldsymbol{i}_t + L_g\frac{d\boldsymbol{i}_t}{dt} + j\omega_m L_g\boldsymbol{i}_t + \boldsymbol{v}_g \tag{13}$$

where R_f and Lf are the inverter-side resistor and inductor; C_f is the capacitor; R_g and L_g denote the grid-side resistor and inductor.

2) Cascaded current and voltage control: The inner current control is applied in the dq-coordinates as

$$\left(\boldsymbol{i}_f^* - \boldsymbol{i}_f\right)\left(k_{ip} + \frac{k_{ii}}{s}\right) + j\omega_0 L_f \boldsymbol{i}_f + \boldsymbol{v}_t = \boldsymbol{v}_o^* \tag{14}$$

where k_{ip} and k_{ii} denote the current control parameters; $\boldsymbol{i}_f^*$ is the current set point; $\boldsymbol{v}_o^*$ is the output voltage set point.

Similarly, the inner voltage control is applied as

$$\left(\boldsymbol{v}_t^* - \boldsymbol{v}_t\right)\left(k_{vp} + \frac{k_{vi}}{s}\right) + j\omega_0 C_f \boldsymbol{v}_t = \boldsymbol{i}_f^* \tag{15}$$

where $\boldsymbol{v}_t^*$ is the capacitor voltage set point.

3) Time delay: Due to the digital implementation and the pulse-width modulation, there is a pure time delay in the VSG. The effect of the time delay can be approximately represented by a low-pass filter with a time constant T_d. This relationship is formulated as

$$\boldsymbol{v}_o = e^{-T_d s}\boldsymbol{v}_o^* \approx \frac{1}{T_d s + 1}\boldsymbol{v}_o^*. \tag{16}$$

4) Virtual impedance: The virtual impedance modifies the capacitor voltage set point as follows:

$$\boldsymbol{v}_t^* = V^* - \boldsymbol{i}_t\left(R_{vir} + j\omega_0 L_{vir}\right) \tag{17}$$

where R_{vir} and L_{vir} denote the virtual resistor and inductor.

5) APC and RPC: VSG's APC and RPC is already formulated as (6) and (7). It is worth mentioning that the d-axis used for the cascaded current and voltage control is oriented to the VSG's phase angle θ_m. This angle is formulated as

$$\theta_m = \int \omega_m. \tag{18}$$

6) Power calculation: VSG's instantaneous output power is calculated as follows:

$$\boldsymbol{S} = P + jQ = \frac{3}{2}\boldsymbol{v}_t\bar{\boldsymbol{i}_t} \tag{19}$$

where $\bar{\boldsymbol{i}_t}$ is the conjugate values of the grid-side current $\boldsymbol{i}_t$.

From(6), (7), and (11)-(19), a 15th-order nonlinear model can be derived to represent the VSG. Applying linearization around the equilibrium point, we have a model as

$$\Delta\dot{\mathbf{x}} = \mathbf{A}\Delta\mathbf{x} + \mathbf{B}\mathbf{u} \tag{20}$$

where the state vector $\mathbf{x}$ and the input vector $\mathbf{u}$ are

$$\begin{aligned}\Delta\mathbf{x} = [&\Delta i_{fd}\ \Delta i_{fq}\ \Delta v_{td}\ \Delta v_{tq}\ \Delta i_{td}\ \Delta i_{tq}\ \Delta v_{od}\ \Delta v_{oq}\\ &\Delta\zeta_d\ \Delta\zeta_q\ \Delta\gamma_d\ \Delta\gamma_q\ \Delta x_{V^*}\ \Delta\omega_m\ \Delta\theta_m]^{\mathrm{T}},\end{aligned} \tag{21}$$

$$\Delta\mathbf{u} = [\Delta P^* \Delta Q^*]^{\mathrm{T}} \tag{22}$$

where the states $\Delta\zeta_d$, $\Delta\zeta_q$, $\Delta\gamma_d$, $\Delta\gamma_q$ and Δx_{V^*} correspond to the integrator in current, voltage and RPC loops, respectively.

III. Accuracy Assessment

In this section, the small-signal models derived in Section II are used for the accuracy assessment. VSG's parameters used in the assessment are presented in Table III. Among these parameters, T_s is the sampling period which corresponds to a switching frequency of 2 kHz, and T_d is set to $1.5T_s$.

Table I
The VSG Parameters

Symbol	Values	Symbol	Values	Symbol	Values
S_{base}	1 MVA	V_n	$690\sqrt{2}/\sqrt{3}$ V	ω_0	314 rad/s
R_f	0.006 pu	L_f	0.12 pu	C_f	0.2 pu
R_g	0.014 pu	L_g	0.14 pu	T_s	0.0005 s
T_d	$1.5T_s$	k_{ip}	0.155	k_{ii}	15
k_{vp}	0.15	k_{vi}	120	R_{vir}	0.01 pu
L_{vir}	0.1 pu	k_{Qp}	0.5 pu	k_{Qi}	0.3 pu
J	30 pu	D	50 pu		

Note: The base value of k_{Qp} and k_{Qi} is V_n/S_{base}, and that of D and J is S_{base}/ω_0.

A. Test system and test cases

The test system is shown in Fig. 3. It is a variant of the three-machine-infinite-bus system in [15]. The infinite bus in the original system is replaced by a 5-bus external grid, and one synchronous generator is replaced by the VSG. The test system is applied in the Digsilent/Powerfactory for the assessment.

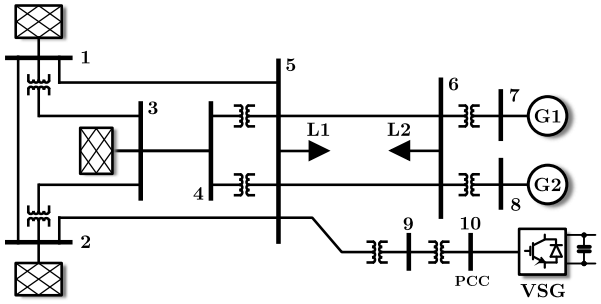

Figure 3. Single-line diagram of the test system.

In the assessment, the short circuit ratio (SCR) is used to characterize the grid strength, and the grid-side resistor and inductor under different SCRs are calculated as [16]:

$$SCR = \frac{V_g^2}{\boldsymbol{Z}_g S_{base}}. \tag{23}$$

Three equilibrium points are considered, and they are i) E1: $P=0.95$ pu and $Q=0$ pu; ii) E2: $P=0.45$ pu and $Q=0$ pu; iii) E3: $P=0.05$ pu and $Q=0$ pu. Two perturbations in the power set points are tested: i) $\Delta P=0.05$ pu; ii) $\Delta Q=0.05$ pu.

B. Case I: SCR is equal to 3

The SCR is firstly set to 3 for a weak grid. Subsequently, the dominant eigenvalues of the RSM and FSM considering three equilibrium points are calculated and shown in Fig. 4. From Fig. 4(a), the FSM has three dominant eigenvalues. The RSM $\Delta P/\Delta P^*$ introduces three dominant eigenvalues as well, and the RSM $\Delta Q/\Delta Q^*$ leads to one real dominant eigenvalue. It is worth noting that, the corresponding eigenvalues are not far away from each other, which indicates a identical-level response. Especially, with the equilibrium point moving from E1 to E3, the differences between RSM and FSM are becoming negligible, as shown in Fig. 4(c).

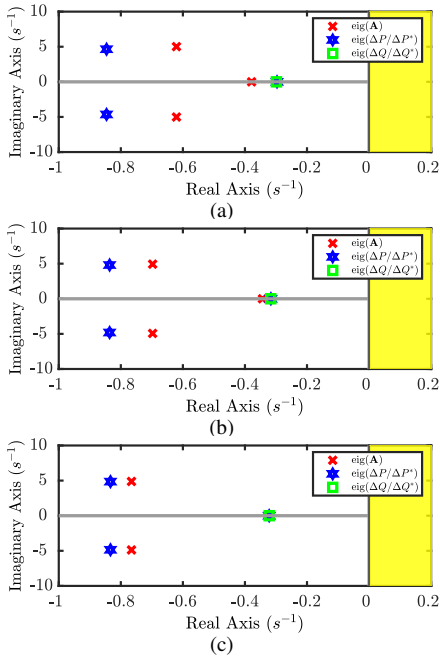

Figure 4. Dominant eigenvalues of the FSM and RSM considering different equilibrium points when SCR is 3: (a) E1; (b) E2; (c) E3.

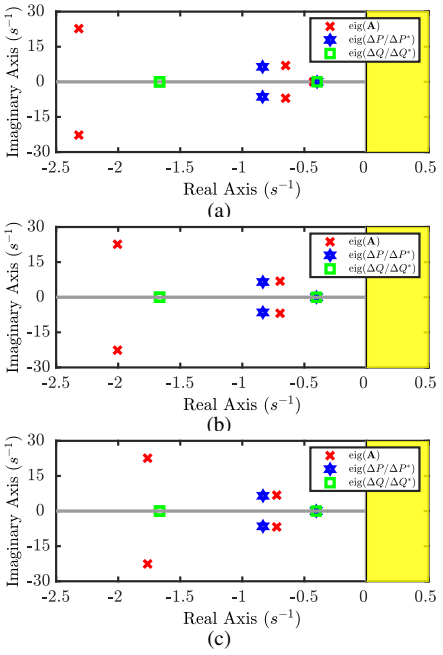

Figure 6. Dominant eigenvalues of FSM and RSM considering different equilibrium points when SCR is 7.

Afterwards, the response of the RSM and FSM are compared with the simulation results (i.e., NM). As presented in Fig. 5, the responses of the active power P and reactive power Q are almost the same when the equilibrium point changes; however, compared with the RSM, the FSM is able to show some reactive-power oscillations in the NM.

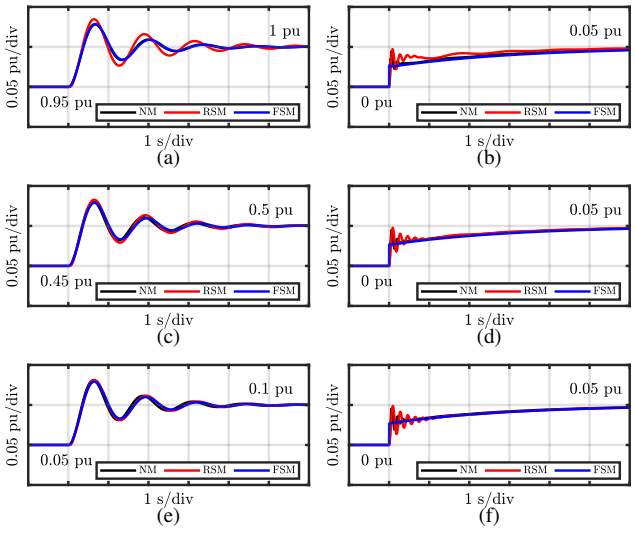

Figure 5. Responses of NM, RSM and FSM when SCR is 3: (a) P around E1; (b) Q around E1; (c) P around E2; (d) Q around E2; (e) P around E3; (f) Q around E3.

C. Case II: SCR is equal to 7

In this study case, the SCR is set to 7, which leads to a relatively strong grid. Then, the dominant eigenvalues of the RSM and FSM considering different equilibrium points are shown in Fig. 6. It can be observed that, different from Case I, where the SCR is set to 3, the FSM has five dominant eigenvalues, and the RSM $\Delta Q/\Delta Q^*$ introduces one more real eigenvalue. As the equilibrium point moves from E1 to E3, two newly-introduced two eigenvalues of the FSM move towards the imaginary axis; however, they are still the most far away from the imaginary axis. The rest eigenvalues of the RSM and FSM shift towards each other. This tendency means that the RSM and FSM will have similar results, but the FSM contains more oscillations at the same time.

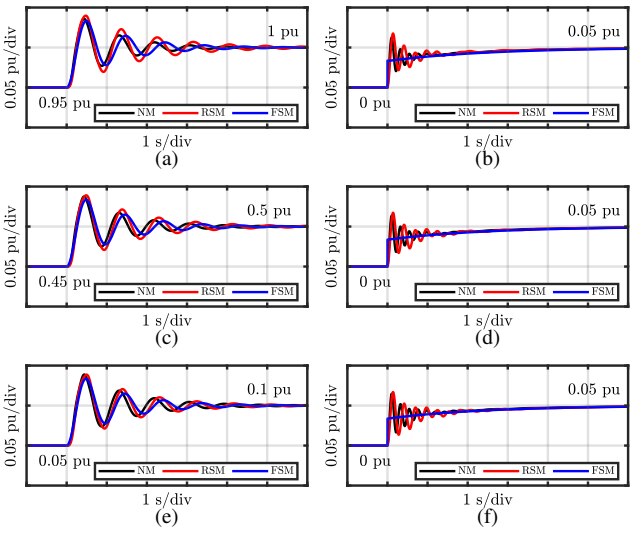

Figure 7. Responses of NM, RSM and FSM when SCR is 7: (a) P around E1; (b) Q around E1; (c) P around E2; (d) Q around E2; (e) P around E3; (f) Q around E3.

The response comparison between NM, RSM and FSM are presented in Fig. 7. As it can be seen, the active power responses are almost the same when different equilibrium points are tested. Regarding the reactive power responses, the results around different equilibrium points share strong similarities as well, except for some oscillations during the transient. Compared with the results in Case I, those oscillations become intensive, which is mainly due to the two newly introduced dominant eigenvalues.

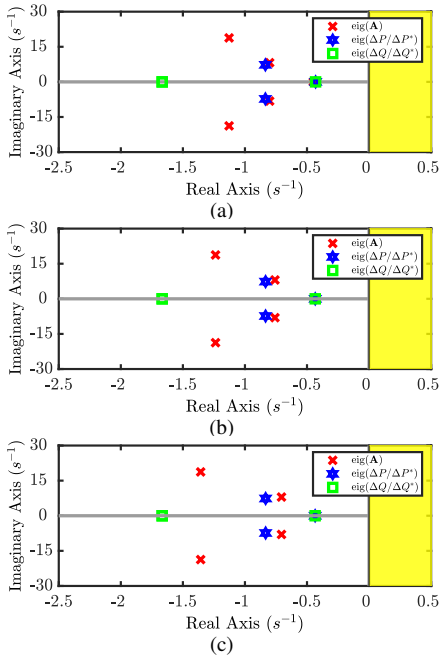

Figure 8. Dominant eigenvalues of FSM and RSM considering different equilibrium points when SCR is 11: (a) E1; (b) E2; (c) E3.

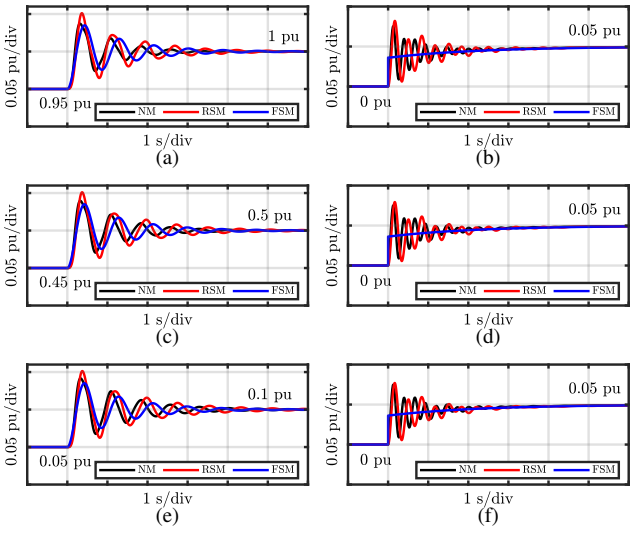

Figure 9. Responses of NM, RSM and FSM when SCR is 11: (a) P around E1; (b) Q around E1; (c) P around E2; (d) Q around E2; (e) P around E3; (f) Q around E3.

D. *Case III: SCR is equal to* 11

Afterwords, the SCR is changed to 11, and the corresponding eigenvalue placement is shown in Fig. 8. As in Case II, the number of each model's dominant eigenvalues is not changed; however, compared with the eigenvalue placement in Case II, the location of FSM's two eigenvalue which has the lowest damping ratio moves further to the imaginary axis. Thus, their effect becomes more significant. The results in Fig. 9 validate this tendency as well. As depicted in Fig. 9, the results of the active power are similar, except for some slight differences in the oscillation frequency. NM and FSM show more intensive oscillations in the reactive power, and the RSM fails to show these oscillations in VSG's RPC.

E. *Case IV: SCR is equal to* 16

When the SCR continues increasing to 16, the impacts of FSM's two poorly-damped eigenvalues are now more significant, especially when the VSG works around the equilibrium point E1. As shown in Fig. 10, these two poorly-damped eigenvalues are closer to the imaginary axis. In this manner, the RSM may fail to provide enough accuracy for a stability analysis. The responses shown in Fig. 11 validate this assumption. As depicted in Fig. 10(a), when the VSG operates around the equilibrium point E1, VSG's APC and RPC exhibit long-time oscillations after a perturbation. The FSM is still able to show the similar results, and it indicates a great modeling accuracy. It is also worth noting that, when the equilibrium point moves from E1 to E3, these two eigenvalues become more stable quickly. Then, less oscillations in the results can be found.

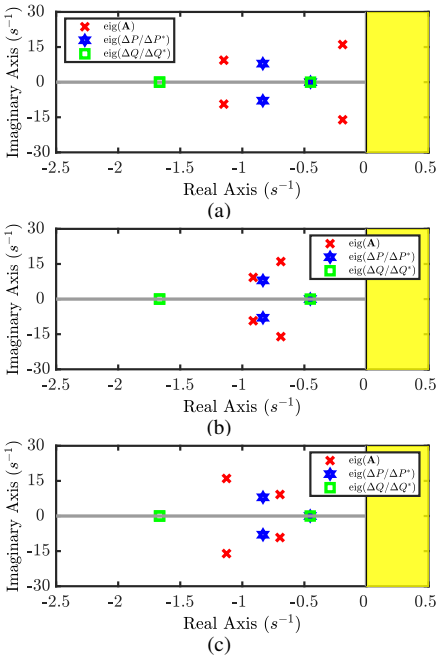

Figure 10. Dominant eigenvalues of FSM and RSM considering different equilibrium points when SCR is 16: (a) E1; (b) E2; (c) E3.

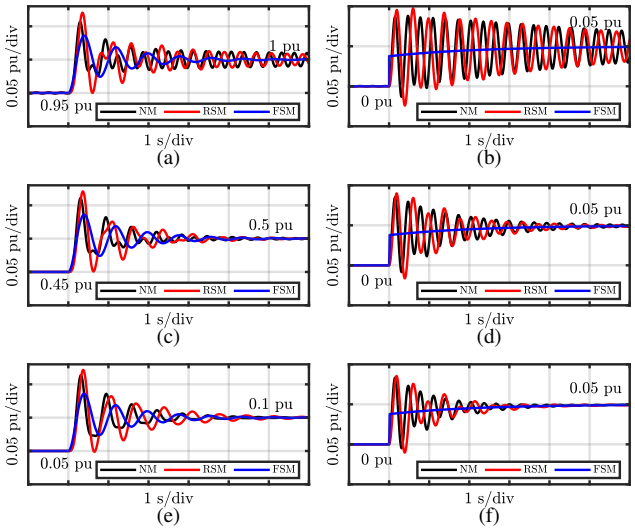

Figure 11. Responses of NM, RSM and FSM when SCR is 16: (a) P around E1; (b) Q around E1; (c) P around E2; (d) Q around E2; (e) P around E3; (f) Q around E3.

IV. Conclusion

In this paper, the modeling accuracy of VSG's two well-known small-signal models has been evaluated under different grid strength cases. Via the eigenvalue analysis and simulation studies, it has been found that the RSM has enough accuracy for the stability analysis under the week or relatively strong grids. With respect to the FSM, it provides better stability and damping-level information when the grid is getting extremely strong; however, compared with the NM, the FSM is still not accurate enough to show the same responses. Moreover, through the comparison around different equilibrium points, it has been revealed that the difference between the RSM and FSM will become smaller when the VSG injects less power into the grid.

References

[1] B. Mohandes, M. S. E. Moursi, N. Hatziargyriou, and S. E. Khatib, "A review of power system flexibility with high penetration of renewables," *IEEE Trans. Power Syst.*, vol. 34, no. 4, p. 3140–3155, Jul. 2019.

[2] H.-P. Beck and R. Hesse, "Virtual synchronous machine," in *Proc. 9th Int. Conf. Elect. Power Qual. Utilisation*, Barcelona, Spain, Oct. 2007, pp. 1–6.

[3] J. Alipoor, Y. Miura, and T. Ise, "Power system stabilization using virtual synchronous generator with alternating moment of inertia," *IEEE J. Emerg. Sel. Topics Power Electron.*, vol. 3, no. 2, pp. 451–458, Jun. 2015.

[4] Q. Zhong and G. Weiss, "Synchronverters: Inverters that mimic synchronous generators," *IEEE Trans. Ind. Electron.*, vol. 58, no. 4, pp. 1259–1267, Apr. 2011.

[5] Y. Cao *et al.*, "A virtual synchronous generator control strategy for VSC-MTDC systems," *IEEE Trans. Energy Convers*, vol. 33, no. 2, pp. 750–761, Jun. 2018.

[6] X. Meng, J. Liu, and Z. Liu, "A generalized droop control for grid-supporting inverter based on comparison between traditional droop control and virtual synchronous generator control," *IEEE Trans. Power Electron.*, vol. 34, no. 6, pp. 5416–5438, Sept. 2019.

[7] J. Liu, Y. Miura, and T. Ise, "Fixed-parameter damping methods of virtual synchronous generator control using state feedback," *IEEE Asses*, vol. 7, pp. 99 177–99 190, Jul. 2019.

[8] J. Liu, Y. Miura, and T. Ise, "A comparative study on damping methods of virtual synchronous generator control," in *2019 21st European Conference on Power Electronics and Applications (EPE '19 ECCE Europe)*, Sept. 2019, pp. 1–10.

[9] Y. Yu, S. K. Chaudhary, G. D. A. Tinajero, L. Xu, N. N. B. A. Bakar, J. C. Vasquez, and J. M. Guerrero, "A reference-feed-forward-based damping method for virtual synchronous generator control," *IEEE Trans. Power Electron.*, vol. 37, no. 7, pp. 7566–7571, Jul. 2022.

[10] M. Chen, D. Zhou, and F. Blaabjerg, "Active power oscillation damping based on acceleration control in paralleled virtual synchronous generators system," *IEEE Trans. Power Electron.*, vol. 36, no. 8, pp. 9501–9510, Aug. 2021.

[11] H. Wu *et al.*, "Small-signal modeling and parameters design for virtual synchronous generators," *IEEE Trans. Ind. Electron.*, vol. 63, no. 7, p. 4292–4303, Jul. 2016.

[12] S. D'Arco, J. A. Suul, and O. B. Fosso, "Automatic tuning of cascaded controllers for power converters using eigenvalue parametric sensitivities," *IEEE Trans. Ind. Appl.*, vol. 51, no. 2, pp. 1743–1753, Sept. 2015.

[13] S. Dong and Y. C. Chen, "Dynamic modelling requirements for tuning of cascaded voltage and current loops in VSMs," in *Proc. 47th Annu. Conf. IEEE Ind. Electron. Soc.*, 2021, pp. 1–6.

[14] Z. Qu, J. C. H. Peng, H. Yang, and D. Srinivasan, "Modeling and analysis of inner controls effects on damping and synchronizing torque components in VSG-controlled converter," *IEEE*, vol. 36, no. 1, pp. 488–499, Mar. 2021.

[15] C. Canizares *et al.*, "Benchmark models for the analysis and control of small-signal oscillatory dynamics in power systems," *IEEE Trans. Power Syst.*, vol. 32, no. 1, pp. 715–722, Jan. 2017.

[16] Q. Liu, T. Caldognetto, and S. Buso, "Stability analysis and auto-tuning of interlinking converters connected to weak grids," *IEEE Trans. Power Electron.*, vol. 34, no. 10, pp. 9435–9446, Oct. 2019.